Journal of The
Electrochemical Society

Unravelling Current–Potential Curves for Au(111) Surface Oxidation in the Presence of Formate

Journal of The Electrochemical Society, 2025 **172** 056506

Unravelling Current–Potential Curves for Au(111) Surface Oxidation in the Presence of Formate

Felix M. Bogenrieder,[1] Johannes M. Hermann,[1] Ludwig A. Kibler,[1,*,z] and Timo Jacob[1,2,3]

[1]*Institute of Electrochemistry, University of Ulm, 89069 Ulm, Germany*
[2]*Helmholtz-Institute Ulm (HIU) for Electrochemical Energy Storage, 89081 Ulm, Germany*
[3]*Karlsruhe Institute of Technology (KIT), 76021 Karlsruhe, Germany*

This study uncovers the dominant voltammetric features of Au(111) surface oxidation in the presence of formate at scan rates of 10 mV s^{-1} and above. The surface oxidation currents are typically masked by the high currents of the formic acid oxidation reaction (FAOR). The presence of formate leads to voltammetric characteristics of Au(111) surface oxidation that are similar to those with (bi)sulfate or acetate, suggesting a common mechanism of Au(111) surface oxidation in the presence of specifically adsorbing oxyanions. This mechanism involves a sequence of surface oxidation processes occurring at surface defects and on terraces. The process of surface oxidation typically commences at monoatomic high steps. Subsequently, the terraces undergo oxidation, which can be described by two additional processes including both adsorption and phase formation via nucleation and growth. The impact of defect density on the voltammetric characteristics of surface oxidation can be modelled and visualized. The simulated voltammograms show features that are well-known for systems such as Au(111) in the presence of (bi)sulfate. These findings contribute to a more profound understanding of the surface oxidation mechanisms on noble metal electrodes and may provide insights that might be important for future studies on interfacial electrochemistry and electrocatalysis.
 [DOI: 10.1149/1945-7111/add4a4]

Manuscript submitted November 5, 2024; revised manuscript received April 28, 2025. Published May 16, 2025.

Gold is unique among other noble metals in its capability to resist the spontaneous formation of bulk oxides under standard conditions. Over the recent decades, extensive research has been dedicated to exploring the electrochemical behavior of gold electrodes, both in their oxide-free state and under various oxidizing conditions.[1–4] The high stability and the straightforward experimental handling of gold electrodes make them suitable model systems for studying the surface oxidation processes of noble metals.

The interaction between water and noble metal electrodes typically leads to an irreversible, multistep formation of different oxidation products, including hydroxides and oxide adlayers, 2D surface oxides, 3D bulk oxides and hydrous oxides.[3,5–7] The kinetics of these processes is strongly influenced by surface defects[8,9] and the presence of specifically adsorbing anions.[3,10,11] Structural changes of the electrode resulting from the surface oxidation or reduction of the oxide layer[8,9,12–15] may give rise to a modification in its electrocatalytic activity.[16–18]

While ordered chemisorbed oxygen overlayers have been observed under ultra-high vacuum (UHV) conditions,[19–21] ordered oxygen overlayers have not been found for electrooxidation of gold surfaces.

Anion adsorption influences both the onset potential of surface oxidation and the kinetics of surface oxidation.[1–3,10,11,22,23] Specifically adsorbing anions, such as sulfate or acetate, lead to one pronounced voltammetric peak for surface oxidation of large Au (111) terraces.[9,14,23–25] A smaller pre-peak is attributed to the oxidation of steps and defects.[24,25] In contrast, the surface oxidation process in the presence of non-specifically adsorbing anions, such as perchlorate, comprises two major peaks. According to the literature, OH adsorption and the subsequent formation of a gold oxide have been proposed as the underlying reason for the occurrence of these two peaks.[1–3,23,26,27] Apparently, surface oxidation leads to the desorption of specifically adsorbed anions [8,28,29] and to place exchange processes between oxygen and gold.[1–3,8,15,23]

Based on the chemical structure and the electrochemical behavior of acetate on Au(111),[22,30] it is possible to derive conclusions for the adsorption of formate on Au(111). Acetate and formate have identical functional groups. Formate is therefore likely to have a similar protective effect to acetate against surface oxidation, by occupying surface sites that would otherwise be available for OH-adsorption (i.e., via competitive adsorption). The Au(111) surface reconstruction is lifted by sulfate and formate at a comparable potential.[4,31] Furthermore, it is known that formate can displace sulfate from the surface and therefore has at least a similar adsorption strength to sulfate.[32–34] It is therefore reasonable to assume that formate adsorbs strongly on the Au(111) surface similar to sulfate or acetate.

A key motivation of our study is the difficulty in directly measuring the voltammetric surface oxidation current of Au(111) in the presence of formic acid, due to the high currents of the formic acid oxidation reaction (FAOR). In contrast to the typically fast adsorption processes[4] which can be disentangled from Faraday currents by probing at high scan rates, surface oxidation cannot be investigated this way due to its sluggish kinetics. This is undoubtedly the case for the FAOR on Au(111).[4,35] Therefore, this paper explores strategies to isolate and study the surface oxidation current under these experimental constraints.

In our previous work, we demonstrated that the kinetics of Au (111) surface oxidation can easily be analyzed with electrochemical techniques despite the superposition with the FAOR as a fast Faraday reaction.[35] This is achieved by measuring current–time curves, which allow for the determination of kinetic parameters of Au(111) surface oxidation (Table I) and hence the surface oxidation current. The oxide-covered gold surface is inactive for the FAOR[4,35] and the deactivation of the electrode surface was employed to derive the kinetics of surface oxidation.

For modelling the chronoamperometric data of Au(111) surface oxidation, three principal contributions are identified,[35] resulting in a relatively simple three-step model to describe the kinetics of surface oxidation. These three processes are assigned to surface oxidation in the vicinity of the step edges (s), oxidation of terraces via adsorption (t), and oxidation of terraces via nucleation and growth (n+g). In addition to the Faraday current, the surface oxidation current itself was included in the model. The exact type of oxide (e.g. hydroxide, oxide, or hydrous oxide) as well as the adsorption or desorption charge of other adsorbates do not play a major role in this simplified model. Furthermore, it is assumed that the FAOR mechanism remains unaltered in the presence of any adsorbed oxygen-

*Electrochemical Society Member.
[z]E-mail: ludwig.kibler@uni-ulm.de

containing species. With these assumptions, the model demonstrates a satisfactory level of agreement with the experimental data.

This study presents the simulation of hypothetical voltammograms for Au(111) surface oxidation in the presence of formate. For comparison, the electrochemical behavior of sulfate, acetate, and perchlorate on Au(111) is considered. While sulfate, acetate, and formate represent a class of specifically adsorbing anions, perchlorate adsorbs more weakly (non-specifically) on the Au(111) surface.[3,30,34,36–38] The nature of the anions exerts a profound influence on the electrochemical behavior of Au(111) as revealed in $j(E)$-curves, both within the double-layer region and particularly in the surface oxidation region, where no Faradaic processes occur.

Experimental

For all measurements, a conventional three-electrode setup was used. The reference electrode was a saturated Mercury/mercurous sulfate electrode (MSE) (SI Analytics), and a graphite rod (⌀3 mm, 99.997%, particle size: 1–5 μm, Goodfellow) served as the counter electrode. Two Au(111) single crystals with different average terrace widths were employed in this study.

One crystal (height 4 mm, diameter 4 mm, 5 N, MaTecK, Jülich, Germany) exhibited a slightly higher surface defect density, whereas the other single crystal (height 5 mm, diameter 4 mm, 5 N, oriented to better than 0.1°, MaTecK, Jülich, Germany) showed a larger mean terrace width as indicated by well-known voltammetric descriptors such as the sulfate spike.[39]

In all figures, the electrode potentials are quoted also against the reversible hydrogen electrode (RHE) since the onset potential of surface oxidation is pH-dependent. Throughout the text, the potential is given vs the RHE unless explicitly stated otherwise.

The cylindrical Au(111) working electrodes were contacted with the electrolyte in a hanging meniscus configuration. Before each measurement, the Au samples were flame-annealed and cooled down in an atmosphere of molecular nitrogen (N5.0). Subsequently, the cleanliness and the quality of the electrochemical system were verified by recording a cyclic voltammogram in the double-layer region. Afterwards, the electrode was rinsed thoroughly with ultrapure water and transferred to another electrochemical cell filled with oxygen-free electrolyte.

The electrolytes were prepared using high-purity sulfuric acid (H_2SO_4), perchloric acid ($HClO_4$), acetic acid (H_3CCOOH), formic acid (HCOOH) (all from Merck, Suprapur), and ultrapure water (18.2 MΩ cm, TOC ⩽ 3 ppb). For all measurements, the electrolytes were purged with nitrogen (N5.0) to remove molecular oxygen from the solution. All measurements were performed using an Autolab PGSTAT302N, which was equipped with the Scan250 and ADC10M modules. The measured current was normalized to the geometrical surface area (0.1257 cm^2).

Results

At constant overpotential, both the FAOR and the Au(111) surface oxidation currents can be described by five independent parameters. A rate constant k_i and a maximum degree of oxide coverage θ_i^{max} are assigned to each of the three processes. Based on the constraint $\theta_s^{max} + \theta_t^{max} + \theta_{n+g}^{max} = 1$, this results in five independent parameters. The rate constants of the simple electrochemical reactions are exponentially dependent on the potential. The maximum degree of coverage resulting from the oxidation in the area of the step edges θ_s^{max} is independent of the potential and only dependent on the defect density of the electrode surface. The maximum coverages θ_t^{max} and θ_{n+g}^{max} are linearly dependent on the potential in the investigated potential range between 0.8 and 0.9 V vs MSE. All kinetic parameters and their respective dependence on the potential are shown in Table I.[35] A comprehensive description of the model can be found in our previous study.[35]

Table I. The dependence of the kinetic parameters $\theta_i^{max}(E)$ and $k_i(E)$ on the electrode potential vs MSE.[35]

$\theta_i^{max}(E) = m_i E + c_i$	$\theta_s^{max}(E)$	$\theta_t^{max}(E)$	$\theta_{n+g}^{max}(E)$
m_i / V^{-1}	0.00	−2.25	2.53
c_i	0.05	2.35	−1.64
$k_i(E) = k_{0,i}10^{b_i E}$	$k_s(E)$ / s^{-1}	$k_t(E)$ / s^{-1}	$k_{n+g}^2(E)$ / s^{-2}
$k_{0,i}$ / s^{-1} or $k_{0,n+g}$ / s^{-2}	$2.09 \cdot 10^{-9}$	$3.42 \cdot 10^{-26}$	$1.10 \cdot 10^{-58}$
b_i / V^{-1}	12.52	27.88	61.94

To a good level of approximation, the surface oxidation current $j^{s.o.}(t, E)$ can be determined from the change in oxide coverage with time $\frac{d\theta(t,E)}{dt}$ multiplied by the charge density $Q_{s.o.}$ related to the transfer of three electrons per Au(111) surface atom, which formally corresponds to one monolayer of Au_2O_3.

$$j^{s.o.}(t, E) = Q_{s.o.}\frac{d\theta(t, E)}{dt} \quad [1]$$

Naturally, the kinetic parameters given in Table I are time-dependent in the course of a voltammetric scan. For a linear sweep, the potential $E(t)$ is varied at a constant scan rate v between two potential limits. Hence, both the maximum coverages $\theta_i^{max}[E]$ and the rate constants $k_i[E]$ are also time-dependent. They are therefore referred to as $\theta_i^{max}(E(t))$ and $k_i(E(t))$, respectively. Within the underlying model for Au(111) surface oxidation, the current density was assumed to be comprised of three important contributions:[35]

$$j^{s.o.}(t, E(t)) = j_s^{s.o.}(t, E(t)) + j_t^{s.o.}(t, E(t)) + j_{n+g}^{s.o.}(t, E(t)) \quad [2]$$

More specifically:

$$\begin{aligned} j^{s.o.}(t, E(t)) = Q_{s.o.}[&\theta_s^{max}(E(t))\, k_s(E(t)) \\ &\exp(-k_s(E(t))t) + \theta_t^{max}(E(t))k_t(E(t)) \\ &\exp(-k_t(E(t))t) + \theta_{n+g}^{max}(E(t)) \\ &2k_{n+g}^2(E(t))t\, \exp(-k_{n+g}^2(E(t))t^2)] \end{aligned} \quad [3]$$

Given the time-dependence of $\theta_i^{max}(E(t))$ and $k_i(E(t))$, the determination of the surface oxidation current is not directly possible using Eqs. 1 and 2. Fortunately, $j^{s.o.}(t, E)$ can be determined by adapting all dependencies of $\theta_i^{max}(E(t))$ with a transformation of variables so that they are exclusively dependent on t and no longer on E.

To calculate the surface oxidation current $j^{s.o.}(t, E(t))$ according to Eq. 3, it is necessary to determine the time-dependence of $\theta_i^{max}(E(t))$. Using the definitions of $\theta_s^{max}(E(t))$ and $\theta_t^{max}(E(t))$, the following equations are obtained:

$$\theta_i(t, E(t)) = \theta_i^{max}(E(t))(1 - e^{-k_i(E(t))t}) \quad [4]$$

$$\begin{aligned} \frac{d\theta_i(t, E(t))}{dt} = (1 - e^{-k_i(E(t))t})\frac{d\theta_i^{max}(E(t))}{dt} - e^{-k_i(E(t))t} \\ \theta_i^{max}\left[-\frac{dk_i(E(t))}{dt}t - k_i(E(t))\right] \end{aligned} \quad [5]$$

In analogy to Eqs. 4 and 5, the following applies to $\theta_{n+g}^{max}(t, E)$:

$$\theta_{n+g}(t, E(t)) = \theta_{n+g}^{max}(E(t))(1 - e^{-k_{n+g}^2(E(t))t^2}) \quad [6]$$

$$\frac{\mathrm{d}\theta_{\mathrm{n+g}}(t,\,E(t))}{\mathrm{d}t} = (1 - \mathrm{e}^{-k^2_{\mathrm{n+g}}(E(t))t^2})\frac{\mathrm{d}\theta^{\max}_{\mathrm{n+g}}(E(t))}{\mathrm{d}t} - \mathrm{e}^{-k^2_{\mathrm{n+g}}(E(t))t^2}\theta^{\max}_{\mathrm{n+g}} \left[-2k_{\mathrm{n+g}}(E(t))\frac{\mathrm{d}k_{\mathrm{n+g}}(E(t))}{\mathrm{d}t}t^2 - 2k^2_{\mathrm{n+g}}(E(t))t\right] \quad [7]$$

To determine $\frac{\mathrm{d}\theta_i(t)}{\mathrm{d}t}$ from $\frac{\mathrm{d}\theta_i(t,E)}{\mathrm{d}t}$, a transformation of variables was carried out for $\theta^{\max}_i(E(t))$ and $k_i(E(t))$. The aim was to replace the dependence on E with a dependence on t so that Eq. 1 can be solved. In general, the following applies to the potential profile $E(t)$ during a linear scan with a constant scan rate $v = \frac{\mathrm{d}E}{\mathrm{d}t}$:

$$E(t) = vt + E_0 \quad [8]$$

As previously demonstrated,[35] $\theta^{\max}_i(E)$ can be approximated linearly within the analyzed potential region. The potential-dependence of $\theta^{\max}_i(E)$ is described by a linear relationship with the slope $m_i = \frac{\mathrm{d}\theta^{\max}_i(E)}{\mathrm{d}E}$ and the intercept $c_i = \theta^{\max}_i(E=0)$.

$$\theta^{\max}_i(E) = m_i E + c_i \quad [9]$$

Both $m_i = \frac{\mathrm{d}\theta^{\max}_i(E)}{\mathrm{d}E}$ and $c_i = \theta^{\max}_i(E=0)$ are constants for the processes (s), (t) and (n+g). The following applies for $\theta^{\max}_i(t)$ using Eqs. 8 and 9:

$$\theta^{\max}_i(t) = m_i(vt + E_0) + c_i \quad [10]$$

$\theta^{\max}_{\mathrm{n+g}}(t)$ can be calculated using the boundary condition (Eq. 11).

$$\theta^{\max}_{\mathrm{n+g}}(t) = 1 - \theta^{\max}_{\mathrm{s}}(t) - \theta^{\max}_{\mathrm{t}}(t) \quad [11]$$

Furthermore, as previously described,[35] the rate constants $k_{\mathrm{s}}(E)$, $k_{\mathrm{t}}(E)$ and $k^2_{\mathrm{n+g}}(E)$ increase exponentially with the potential E. Consequently, the potential-dependence of these constants was assumed using the following simple relationship:

$$k_i(E) = k_{0,i}10^{b_i E} \quad [12]$$

For the processes indexed by (s) and (t), the following applies: $k_{0,i} = k_i(E=0)$ and $b_i = \frac{\mathrm{d}\log_{10}(k_i)}{\mathrm{d}E}$, and similarly for (n+g): $k_{0,\mathrm{n+g}} = k^2_{\mathrm{n+g}}(E=0)$ and $b_{\mathrm{n+g}} = \frac{\mathrm{d}\log_{10}(k^2_{\mathrm{n+g}})}{\mathrm{d}E}$. For $k_{\mathrm{s}}(t)$ and $k_{\mathrm{t}}(t)$, using Eqs. 8 and 12, we have:

$$k_i(t) = k_{0,i}10^{b_i(vt+E_0)} \quad [13]$$

The same applies to $k_{\mathrm{n+g}}(t)$:

$$k^2_{\mathrm{n+g}}(t) = k_{0,\mathrm{n+g}}10^{b_{\mathrm{n+g}}(vt+E_0)} \quad [14]$$

The time-dependence of the maximum oxide coverage $\frac{\mathrm{d}\theta^{\max}_i(t)}{\mathrm{d}t}$ and $\frac{\mathrm{d}\theta^{\max}_{\mathrm{n+g}}(t)}{\mathrm{d}t}$ is determined using Eq. 10 and the condition given in Eq. 11.

$$\frac{\mathrm{d}\theta^{\max}_i(t)}{\mathrm{d}t} = v\frac{\mathrm{d}\theta^{\max}_i(E)}{\mathrm{d}E} \quad [15]$$

$$\frac{\mathrm{d}\theta^{\max}_{\mathrm{n+g}}(t)}{\mathrm{d}t} = -\frac{\mathrm{d}\theta^{\max}_{\mathrm{s}}(t)}{\mathrm{d}t} - \frac{\mathrm{d}\theta^{\max}_{t}(t)}{\mathrm{d}t} \quad [16]$$

For the temporal changes $\frac{\mathrm{d}k_i(t)}{\mathrm{d}t}$ and $\frac{\mathrm{d}k_{\mathrm{n+g}}(t)}{\mathrm{d}t}$ of the rate constants within the potential scan, the following applies based on Eqs. 13 and 14:

$$\frac{\mathrm{d}k_i(t)}{\mathrm{d}t} = \ln(10)k_i(0)b_i v10^{b_i(vt+E_0)} \quad [17]$$

$$\frac{\mathrm{d}k_{\mathrm{n+g}}(t)}{\mathrm{d}t} = \frac{\frac{\mathrm{d}k^2_{\mathrm{n+g}}(t)}{\mathrm{d}t}}{2\sqrt{k^2_{\mathrm{n+g}}(t)}} \quad [18]$$

with

$$\frac{\mathrm{d}k^2_{\mathrm{n+g}}(t)}{\mathrm{d}t} = \ln(10)k_{\mathrm{n+g}}(0)b_{\mathrm{n+g}}v10^{b_{\mathrm{n+g}}(vt+E_0)} \quad [19]$$

Using the time-dependent functions for $\theta^{\max}_i(t)$ (Eq. 10), $\theta^{\max}_{\mathrm{n+g}}(t)$ (Eq. 11), $k_i(t)$ (Eq. 13) and $k^2_{\mathrm{n+g}}(t)$ (Eq. 14) and their time derivatives (Eqs. 15–19), $\frac{\mathrm{d}\theta_i(t)}{\mathrm{d}t}$ can be determined. For a given value of the scan rate v and the initial potential E_0, $\frac{\mathrm{d}\theta_i(t)}{\mathrm{d}t}$ can be obtained for any point in time. To simulate a $j(E)$ curve, a potential $E(t)$ can be assigned to each time t at a constant scan rate v (see Eq. 8). The sum of all the changes in coverage over time determined from Eqs. 5 and 7 can be multiplied by $Q_{\mathrm{s.o.}}$ from Eq. 1 to obtain the surface oxidation current as a function of potential $j^{\mathrm{s.o.}}(E)$.

$$j^{\mathrm{s.o.}}(E) = Q_{\mathrm{s.o.}}\sum\frac{\mathrm{d}\theta_i(E)}{\mathrm{d}t} \quad [20]$$

For a better graphical comparison of current–potential curves at different scan rates, the pseudo capacitance $C_{\mathrm{pseudo}}(E)$ can be used as deduced from $j^{\mathrm{s.o.}}(E)$ using Eq. 21.

$$C_{\mathrm{pseudo}}(E) = \frac{j_{\mathrm{s.o.}}(E)}{v} \quad [21]$$

In Fig. 1 the calculated pseudo-capacitance $C_{\mathrm{pseudo}}(E)$ is plotted vs the potential for different scan rates.

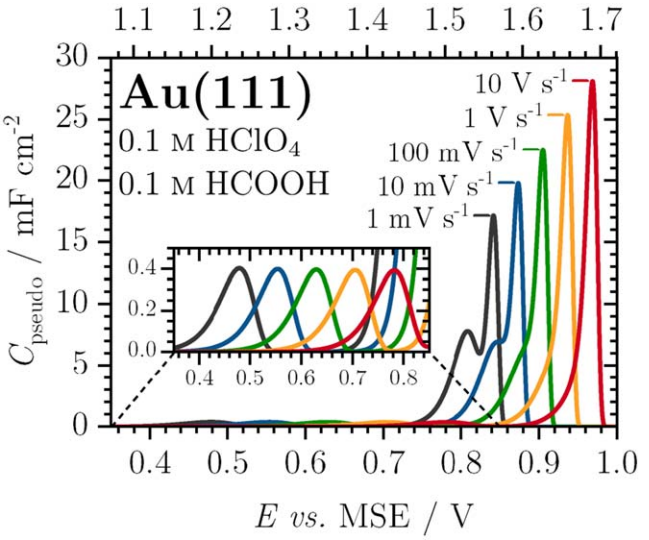

Figure 1. Simulated curves for pseudo-capacitance vs electrode potential for the surface oxidation of Au(111) in 0.1 M $HClO_4$ + 0.1 M HCOOH using the experimental kinetic parameters of our previous study.[35] Scan rates: 10, 1, 0.1, 0.01, and 0.001 V s^{-1}.

The successive contributions to oxide formation at steps (s) and on terraces by adsorption (t) or nucleation and growth kinetics (n+g) are apparent in the plot of the pseudo-capacitance vs potential. Due to the relatively small contribution of the oxidation at surface defects, only a small voltammetric (pre-)peak is discernible. For better illustration, the potential region for surface oxidation at steps is magnified in the inset of Fig. 1. The shape of the peaks in the simulated voltammograms for Au(111) surface oxidation in the presence of formate resembles the $j(E)$ curves for Au(111) in the presence of other specifically adsorbing oxyanions such as sulfate or acetate, as will be discussed below (see Fig. 3). For all the anions used in this study, the peaks for terrace and step oxidation are easily distinguishable. Although formate adsorption and desorption as elementary processes are neglected in the simple kinetic model, the curves shown in Fig. 1 effectively correspond to surface oxidation in the presence of specifically adsorbing formate because the surface oxidation kinetics was investigated under this condition. While the net currents for Au(111) surface oxidation are masked by formic acid oxidation, they can be unveiled and disentangled by the kinetic investigation in the experiment and the subsequent simulation.

The proposed model of Au(111) surface oxidation in the presence of formate[35] is supported by the strong resemblance in shape and position of the voltammetric peaks with those obtained in the presence of sulfate or acetate (cf Figs. 1 and 3). But there are also some caveats. In the simulation, the onset potential of surface oxidation shifts to lower values with decreasing scan rate. For example, the surface oxidation seemingly commences at 1.14 V when scanning with 10 mV s^{-1}. However, according to the experiment, this potential is within the stability range of oxide-free Au (111) in 0.1 M $HClO_4$ + 0.1 M HCOOH.[35] Therefore, the onset potential of Au(111) surface oxidation is only plausible if the scan rate is not chosen to be too low.

The observation originates from the exponential dependence of the rate constants of the surface oxidation (k_{ox}) on potential within the kinetic model over the entire potential range. This entails that the rate constant k_i and thus $j^{s,o,}(E(t))$ never become zero. Therefore, the onset potential of surface oxidation in the presented model systematically shifts to lower potentials as the scan rate v decreases. Of course, the exponential behavior of the apparent rate constant k_i only applies to the experiment at large overpotentials in the context of the Butler-Volmer kinetics. For low overpotentials, the kinetics of Au oxide reduction becomes important. However, this aspect is not incorporated into the present model. Of course, the deviation from the apparent rate constant also influences the oxidation current. In the vicinity of the onset potential of surface oxidation, which is presumably close to its equilibrium potential, the total current j_{total} has to be accounted for as the sum of the two partial currents $j_{total}(E) = j_{ox}(E) + j_{red}(E)$. Neglecting the cathodic partial current in the model leads to larger positive currents with a simple exponential behavior explaining the divergence from experimental curves.

Furthermore, it should be noted that the explicit adsorption of formate is not included in the model. Strongly adsorbing anions protect the oxide-free surface and shift the onset potential positively.[2,3,8,18,22–24,40,41] In the case of weakly adsorbing anions such as perchlorate, this effect is less pronounced, and surface oxidation starts at lower potentials (see Fig. 3).

In the potential region of surface oxidation, a significantly lower coverage of formate is expected,[28,29] compared to potentials just below. The model thus represents a surface with a lower formate coverage in comparison to the coverage positive of the formate phase transition in the falling flank of the bell-shaped curve during the slow formic acid reaction. This also contributes to the onset potential of surface oxidation (equivalent to Au(111) in the presence of perchlorate) being shifted negatively.

So far, a series of hypothetical voltammograms for net surface oxidation in the presence of formate is simulated based on FAOR

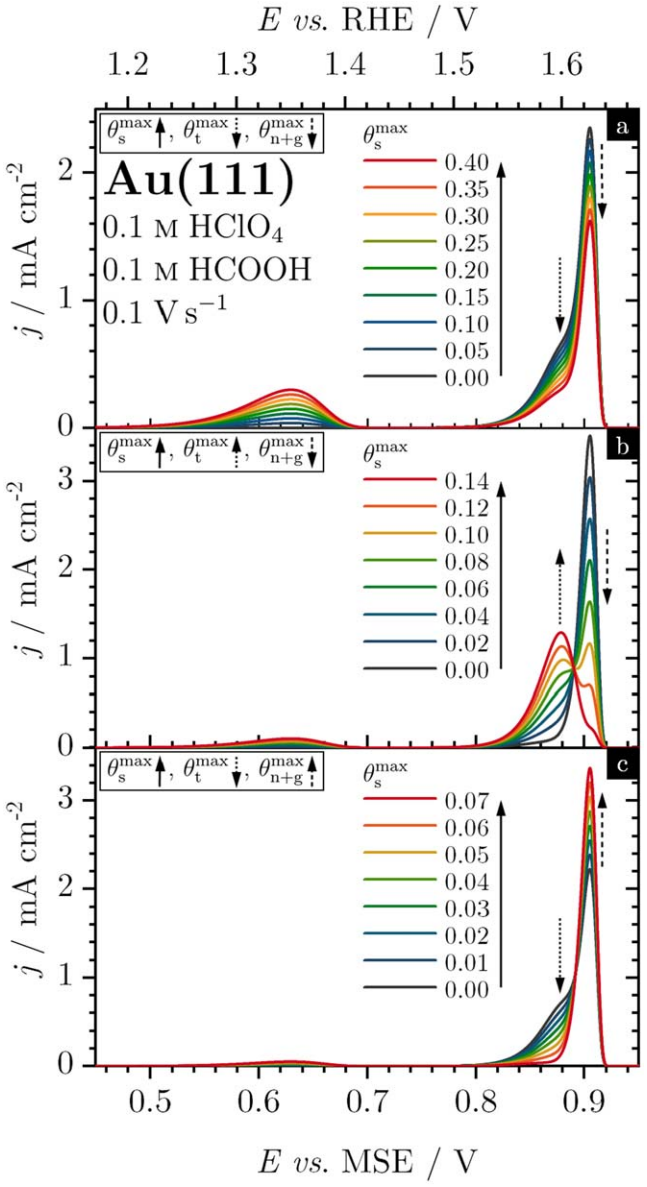

Figure 2. Simulated current–potential curves for Au(111) surface oxidation in 0.1 M $HClO_4$ + 0.1 M HCOOH at a scan rate of 0.1 V s^{-1} for different values of θ_s^{max}. Three possible dependencies of the parameters θ_s^{max}, θ_t^{max} and θ_{n+g}^{max} are depicted in (a)–(c) and marked with arrows. The feasible defect densities, as predicted by the model, are illustrated in a color gradient.

experiments with the same Au(111) electrodes. Interestingly, beyond that, the $j(E)$-curve for an electrode surface of different defect densities can also be simulated. The value of θ_s^{max} can be changed systematically to consider different surface defect densities. According to the boundary condition given in Eq. 11, a change in θ_s^{max} influences the parameters θ_t^{max} and θ_{n+g}^{max}. Basically, θ_t^{max} and θ_{n+g}^{max} can react in three different ways to the variation of θ_s^{max}: An increase in θ_s^{max} can lead (*i*) to a decrease in both θ_t^{max} and θ_{n+g}^{max} while their ratio stays independent of θ_s^{max} for simplicity (Fig. 2a). Alternatively, an increase in θ_s^{max} can lead (*ii*) to an increase in θ_t^{max} and a decrease in θ_{n+g}^{max} (Fig. 2b) or (*iii*) to a decrease in θ_t^{max} and increase of θ_{n+g}^{max} (Fig. 2c). Assuming that the potential dependence of the individual processes occurring on terraces is independent of the defect density, the parameter m_i in Eq. 9 and $k_i(E)$ in Eq. 12 can be considered as constant. A change in θ_s^{max} will therefore mainly affect the parameter c_i in Eq. 9.

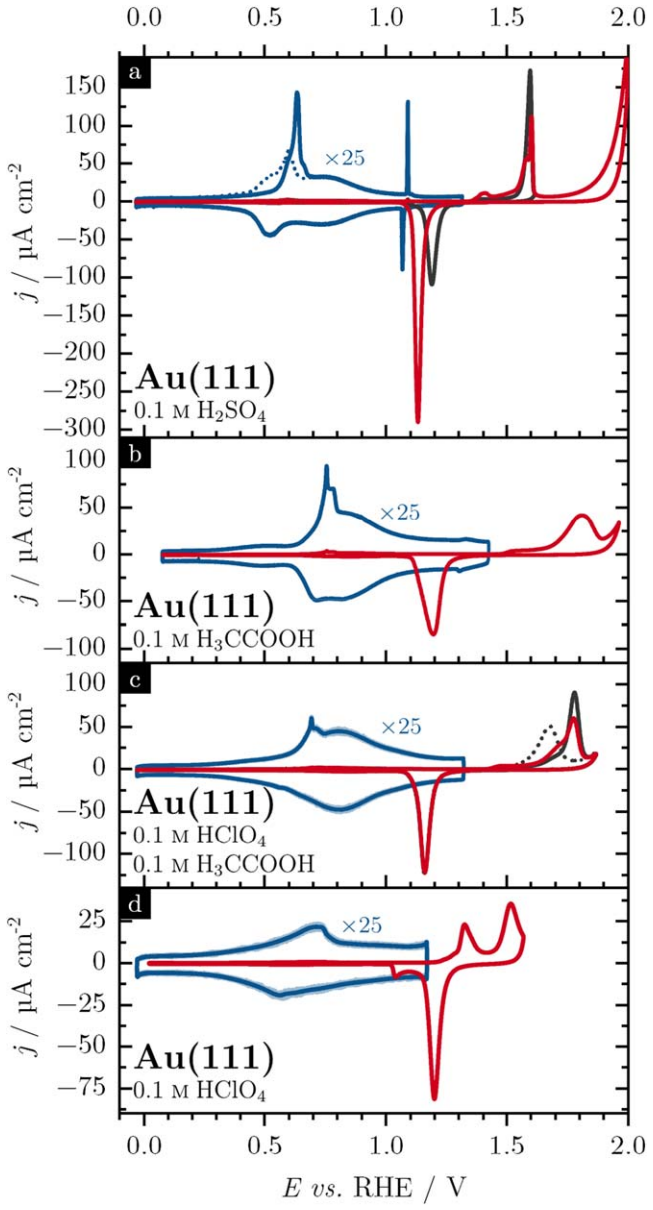

Figure 3. Current-potential curves for Au(111) in (a) 0.1 M H_2SO_4, (b) 0.1 M H_3CCOOH, (c) 0.1 M $HClO_4$ + 0.1 M H_3CCOOH and (d) 0.1 M $HClO_4$ with a scan rate of 10 mV s^{-1}. The double-layer region (blue curves) is enlarged by a factor of 25. The second cycles are shown as a dotted line. To illustrate the influence of the surface defect density on the currents in the region of surface oxidation, two single crystals with different average terrace widths are shown. The crystal corresponding to the black curve exhibits a significantly higher sulfate spike, which indicates a larger mean terrace width.[39] All potentials were corrected by the IR drop.

In case (*i*), a change in c_s has an equivalent impact on both c_t and c_{n+g}. By contrast, in case (*ii*), the opposing trend of c_t and c_{n+g} applies, which has been discovered in our previous study[35] for two single crystals of different surface quality. Finally, concerning case (*iii*), the trend of case (*ii*) is inverted. It is important to notice that all three approaches are designed to provide a quick qualitative comparison of the simulated voltammetric curves. The resulting overview of simulating varying defect densities for all three methods is illustrated in Fig. 2.

The current–potential curves depicted in Figs. 2a–2c demonstrate the strong impact of defect density on the region of Au(111) terrace oxidation. Regardless of θ_s^{max}, all three processes of surface oxide formation can easily be discerned in the simulated voltammogram (Fig. 2). While Fig. 2a demonstrates case (*i*) with a decrease in both θ_t^{max} and θ_{n+g}^{max}, Figs. 2b and 2c illustrate the contrasting trends of case (*ii*) and (*iii*), respectively. The resulting hypothetical current–potential curves can nicely be compared with the experimental voltammograms for Au(111) in the presence of non-oxidizable anions such as sulfate and acetate. In this way, the simulation method can be tested for plausibility.

Figures 3a–3d illustrate the current–potential curves for Au(111) both in the double-layer region and the surface oxidation in the following electrolytes: (a) 0.1 M H_2SO_4, (b) 0.1 M H_3CCOOH, (c) 0.1 M $HClO_4$ + 0.1 M H_3CCOOH and (d) 0.1 M $HClO_4$. The current in the double-layer region is depicted in blue and magnified by a factor of 25. The two strongly adsorbing anions, sulfate and acetate, exhibit comparable characteristics in both the double-layer region and the surface oxidation regime. In contrast to non-specifically adsorbing perchlorate, the onset potential of surface oxidation is shifted to significantly more positive potentials in the presence of the specifically adsorbing anions. The surface oxidation region in the presence of strongly adsorbing anions is composed of a (small) pre-peak corresponding to oxide formation on defects and steps and a main peak corresponding to oxide formation on terraces. In contrast, Au(111) surface oxidation in the presence of perchlorate consists of two distinct peaks that are relatively independent of the surface defect density. The former peak has at least two shoulders,[2,40] which in turn depend strongly on the surface quality (not shown). So far, the significantly different current–potential curves observed in the presence of specifically or non-specifically adsorbing anions have been attributed to different mechanisms of oxide formation.[2,3,8,9,23–25,40–43] However, an in situ scanning tunneling microscopy study has shown that the initial process of surface oxidation is related to oxidation of the steps and defects in the presence of both specifically and non-specifically adsorbing anions.[43] In the case of perchlorate, the formation of a (sub) monolayer of an oxide species between adsorbed perchlorate cannot be excluded according to the literature.[40,41]

As with perchloric acid, the initial process of surface oxidation in the presence of sulfate has been attributed to the oxidation of steps and defects.[8,25] The height of the main oxidation peak increases with the average Au(111) terrace width.[24] The shoulder around 1.7 V discernible in the second cycle of terrace oxidation in the precence of acetate (Fig. 3c) can also be attributed to a process occurring on the terraces.[9] During this process, small rough areas were formed on the terraces, which only grew when the potential of the main oxidation peak was reached.[9]

The onset potential of Au(111) surface oxidation is highest in the presence of acetate compared to the other anions investigated. During the oxidation of the surface, adsorbed acetate is gradually displaced from the surface.[22] Compared to the displacement of sulfate, acetate desorption takes place in a wider potential range. This indicates a strong interaction between the Au(111) surface and the adsorbed acetate anions. The similarity of the voltammetric curves suggests the same surface oxidation mechanism of Au(111) in the presence of sulfate and acetate. Furthermore, the charge associated with the oxidation of surface defects is similar in both cases, with approximately 5% of the charge for the formation of a complete monolayer of Au_2O_3. This indicates that the nature of the anion, whether sulfate or acetate, does not significantly affect the extent of the oxidation process at surface defects.

Voltammetric curves reveal obvious similarities for Au(111) surface oxidation in the presence of formate (Fig. 1), sulfate (Fig. 3a), and acetate (Fig. 3b+c). This points towards a similar adsorption strength[32–34] and a common surface oxidation mechanism. A general mechanism of Au(111) surface oxidation is therefore assumed for all investigated specifically adsorbing oxyanions.

In addition, the influence of the surface defect density on the current–potential curves for Au(111) oxidation is demonstrated in Fig. 3. In Figs. 3a and 3c, two crystals of differing surface quality

were employed in order to investigate the impact of defect density on the current–potential curves. The crystal corresponding to the black curve exhibits a significantly higher sulfate spike, which indicates a larger mean terrace width.[39] At higher defect densities, the curves in Figs. 3a and 3c show a decrease in the main oxidation peak and an increase in the pre-peak. This effect is even more pronounced when comparing the first and second cycles of surface oxidation in Fig. 3c. In general, repeated oxidation and reduction of the surface leads to an increased defect density.[8,14] In the second cycle of surface oxidation (dotted curve in Fig. 3c), the main terrace oxidation peak is no longer visible. The process, previously forming only a shoulder, now becomes the main peak.

A similar voltammetric behavior is seen in Fig. 2b for Au(111) surface oxidation in the presence of formate, while the curves shown in Figs. 2a and 2c represent a different behavior. This demonstrates that as the maximum oxide coverage at surface steps θ_s^{max} increases for Au(111) surface oxidation in the presence of formate, θ_{n+g}^{max} decreases, while θ_t^{max} increases. A similar conclusion was reached in our previous publication,[35] and the curves presented here further corroborate this finding. While the charge of the first process of surface oxidation at 0.615 V vs MSE increases with increasing surface defect density, the net charge for the processes associated with oxide formation on terraces decreases. This is in agreement with previously published data for the surface oxidation of stepped single crystals by Štrbac et al.,[24] indicating that the underlying mechanism matches across different defect densities and crystallographic orientations.[44] In summary, case (*ii*) or Fig. 2b fits best the effect of defect density on the surface oxidation voltammograms.

Although the formate adsorption charge is ignored in our simple model, the specific adsorption of formate protects the surface from oxidation. This protective effect influences the kinetics of surface oxidation. The simulated $C(E)$ curves resemble those of Au(111) surface oxidation in the presence of other specifically adsorbing anions such as sulfate or acetate (see Fig. 3). Again, the similar adsorption strength of sulfate and formate is retrieved. Due to the obvious limitations of the model as described above, the $C(E)$ curves can only be compared with the voltammetric peaks for surface oxidation in the presence of sulfate or acetate at scan rates $v > 10$ mV s^{-1}.

Furthermore, a kinetic coupling between the processes in the model has not been considered. Such coupling might be a reason for the experimentally observed current in the potential region between the oxidation of defects and terraces. Notably, the current in this potential region is negligible for high-quality surfaces. Consequently, the simulated current–potential curves are representative of high-quality Au(111) electrodes.

The application of the model with the three main contributions of oxide formation at steps, on terraces, and surface oxidation by nucleation and growth to simulate $C(E)$ curves emphasizes the validity of the assumptions made in the model.[35] Although anion adsorption, double-layer charging, and the chemical nature of oxygen species other than the final two-dimensional Au_2O_3 surface oxide has been neglected in the model, the model reproduces well both the onset potential of surface oxidation (compared to Au(111) in 0.1 M $HClO_4$) as well as the peak shape and position (compared to Au(111) in 0.1 M H_2SO_4 or H_3CCOOH). For scan rates $v > 10$ mV s^{-1}, the model is therefore suitable for describing the processes during surface oxidation in the presence of formate, especially for well-ordered single-crystal surfaces. The surface oxidation currents masked by the FAOR are not directly accessible and can be elucidated and revealed by utilizing the FAOR as a probe reaction. The $C(E)$ curves suggest a surface oxidation mechanism similar to that in the presence of specifically adsorbing anions such as sulfate or acetate. The oxide formation on the step edges is separated from the oxide formation on the terraces. The main oxidation peak corresponds to oxide formation on the terraces. The formate layer protects the terraces from surface oxidation and therefore probably has a similar adsorption strength as sulfate or acetate.

Conclusions

In this study, we uncovered the Au(111) surface oxidation current from the simultaneous formic acid oxidation reaction (FAOR) current. Our findings provide significant insights into the surface oxidation mechanism in the presence of formate, offering a deeper understanding of the underlying processes.

The Au(111) surface oxidation mechanism bears a close resemblance to the oxidation with other specifically adsorbing anions. This mechanism comprises two primary components: oxidation in the vicinity of the step edges and oxidation on the terraces. The oxidized area in the vicinity of the steps is predominantly influenced by the electronic structure of the metallic surface, indicating the critical role of the surface's atomic configuration in oxidation processes.

Furthermore, the protective effect of different anions against surface oxidation can be ranked in the following order: acetic acid (H_3CCOOH) > sulfuric acid (H_2SO_4) > perchloric acid ($HClO_4$). This hierarchy demonstrates the varying degrees of surface protection provided by different anions. Our results elucidate the complex interplay between adsorbed anions and the Au(111) surface oxidation mechanism in the presence of formate. These insights contribute to a deeper understanding of the oxidation processes and may inform future studies on surface chemistry and catalysis.

Considering the findings presented here, we propose two promising avenues for further investigation. Firstly, we propose the development of a simple methodology for the determination of kinetic constants from cyclic voltammetry data. This approach involves measuring cyclic voltammetry at several scan rates, which can then be used to fit a model and extract the kinetic constants and defect density. This advancement could facilitate a straightforward and efficient measurement of reaction kinetics in surface oxidation studies. Secondly, to further verify our findings, we propose the use of stepped single crystals to examine the dependency of θ_t^{max} and θ_{n+g}^{max} on θ_s^{max} to further refine the proposed model.

By advancing these areas of research, we aim to deepen our understanding of surface oxidation processes of noble metals in general.

Acknowledgments

The authors gratefully acknowledge funding by the DFG (Deutsche Forschungsgemeinschaft) through project 501805371 and the collaborative research center TRR-234 (project no. 364549901). Further, support by the BMBF (Bundesministerium fur Bildung *u*nd Forschung) through the project CASINO (FKZ: 03XP0487G) and the state of Baden-Württemberg and the DFG through grant no INST 40/574–1 FUGG is acknowledged. Felix M. Bogenrieder: Visualization, Validation, Investigation, Formal analysis, Data curation, Conceptualization, Writing—original draft preparation. Johannes M. Hermann: Supervision, Writing—review & editing. Ludwig A. Kibler: Supervision, Conceptualization, Writing—review & editing. Timo Jacob: Funding acquisition, Project administration, Resources, Supervision, Writing—review & editing.

ORCID

Felix M. Bogenrieder https://orcid.org/0000-0002-2266-4321
Johannes M. Hermann https://orcid.org/0000-0001-7119-1295
Ludwig A. Kibler https://orcid.org/0000-0003-1152-1445
Timo Jacob https://orcid.org/0000-0001-7777-2306

References

1. D. Dickertmann, J. W. Schultze, and K. J. Vetter, *J. Electroanal. Chem.*, **55**, 429 (1974).
2. H. Angerstein-Kozlowska, B. E. Conway, A. Hamelin, and L. Stoicoviciu, *Electrochim. Acta*, **31**, 1051 (1986).
3. B. E. Conway, *Prog. Surf. Sci.*, **49**, 331 (1995).
4. L. A. Kibler and M. Al-Shakran, *J. Phys. Chem. C*, **120**, 16238 (2016).
5. R. Bradley Shumbera, H. H. Kan, and J. F. Weaver, *Surf. Sci.*, **601**, 4809 (2007).
6. L. D. Burke and M. E. G. Lyons, "Electrochemistry of Hydrous Oxide Films." *Modern Aspects of Electrochemistry*, ed. R. E. White, J. O'M Bockris, and B. E. Conway (Springer, Boston, MA) 18169 (1986).

7. L. D. Burke and P. F. Nugent, *Gold Bull.*, **30**, 43 (1997).
8. U. Zhumaev, A. V. Rudnev, J.-F. Li, A. Kuzume, T.-H. Vu, and T. Wandlowski, *Electrochim. Acta*, **112**, 853 (2013).
9. M. A. Schneeweiss and D. M. Kolb, *Solid State Ionics*, **94**, 171 (1997).
10. F. J. Rodríguez Nieto, G. Andreasen, M. E. Martins, F. Castez, R. C. Salvarezza, and A. J. Arvia, *J. Phys. Chem. B*, **107**, 11452 (2003).
11. G. N. Van Huong, C. Hinnen, and J. Lecoeur, *J. Electroanal. Chem. Interfacial Electrochem.*, **106**, 185 (1980).
12. C. Köntje, D. M. Kolb, and G. Jerkiewicz, *Langmuir*, **29**, 10272 (2013).
13. R. J. Nichols, O. M. Magnussen, J. Hotlos, T. Twomey, R. J. Behm, and D. M. Kolb, *J. Electroanal. Chem. Interfacial Electrochem.*, **290**, 21 (1990).
14. T. Kondo, J. Morita, K. Hanaoka, S. Takakusagi, K. Tamura, M. Takahasi, J. Mizuki, and K. Uosaki, *J. Phys. Chem. C*, **111**, 13197 (2007).
15. T. Kondo, J. Zegenhagen, S. Takakusagi, and K. Uosaki, *Surf. Sci.*, **631**, 96 (2015).
16. T. Lim and J. Kim, *J. Korean Chem. Soc.*, **60**, 310 (2016).
17. M. M. Elnagar, J. M. Hermann, T. Jacob, and L. A. Kibler, *Electrochim. Acta*, **372**, 137867 (2021).
18. A. Hamelin, Y. Ho, S. C. Chang, X. Gao, and M. J. Weaver, *Langmuir*, **8**, 975 (1992).
19. C. Jianming, W. Naijuan, Q. Shangxue, F. Kean, and M. S. Zei, *Chinese Phys. Lett.*, **6**, 92 (1989).
20. L. Huang, J. Chevrier, P. Zeppenfeld, and G. Cosma, *Appl. Phys. Lett.*, **66**, 935 (1995).
21. J. Chevrier, L. Huang, P. Zeppenfeld, and G. Comsa, *Surf. Sci.*, **355**, 1 (1996).
22. B. Braunschweig, P. Mukherjee, R. B. Kutz, A. Wieckowski, and D. D. Dlott, *J. Chem. Phys.*, **133**, 234702 (2010).
23. H. Angerstein-Kozlowska, B. E. Conway, A. Hamelin, and L. Stoicoviciu, *J. Electroanal. Chem.*, **228**, 429 (1987).
24. S. Štrbac, R. R. Adžić, and A. Hamelin, *J. Electroanal. Chem. Interfacial Electrochem.*, **249**, 291 (1988).
25. M. A. Schneeweiss, D. M. Kolb, D. Liu, and D. Mandler, *Can. J. Chem.*, **75**, 1703 (1997).
26. H. Honbo, S. Suga, and K. Itaya, *Anal. Chem.*, **62**, 2424 (1990).
27. G. J. Edens, X. Gao, M. J. Weaver, N. M. Markovic, and P. N. Ross, *Surf. Sci.*, **302**, L275 (1994).
28. Z. Jusys and R. Jürgen Behm, *ECS Trans.*, **66**, 1 (2015).
29. Z. Jusys and R. J. Behm, *J. Electroanal. Chem.*, **800**, 60 (2017).
30. A. Abdelrahman, J. M. Hermann, T. Jacob, and L. A. Kibler, *ChemPhysChem*, **20**, 2989 (2019).
31. J. M. Hermann, A. Abdelrahman, T. Jacob, and L. A. Kibler, *Electrochim. Acta*, **347**, 136287 (2020).
32. S. Chen, B. Wu, and C. Cha, *J. Electroanal. Chem.*, **431**, 243 (1997).
33. S. Brimaud, J. Solla-Gullón, I. Weber, J. M. Feliu, and R. J. Behm, *Chem. Electro. Chem*, **1**, 1075 (2014).
34. J. M. Hermann, A. Abdelrahman, T. Jacob, and L. A. Kibler, *Electrochim. Acta*, **385**, 138279 (2021).
35. F. M. Bogenrieder, J. M. Hermann, L. A. Kibler, and T. Jacob, *J. Electrochem. Soc.*, **169**, 116513 (2022).
36. F. Silva and A. Martins, *Electrochim. Acta*, **44**, 919 (1998).
37. O. M. Magnussen, *Chem. Rev.*, **102**, 679 (2002).
38. D. V. Tripkovic, D. Strmcnik, D. van der Vliet, V. Stamenkovic, and N. M. Markovic, *Faraday Discuss.*, **140**, 25 (2008).
39. T. H. Dretschkow and T. H. Wandlowski, *Berichte der Bunsengesellschaft für Phys. Chemie*, **101**, 749 (1997).
40. A. Hamelin, *J. Electroanal. Chem.*, **407**, 1 (1996).
41. A. Hamelin and A. M. Martins, *J. Electroanal. Chem.*, **407**, 13 (1996).
42. H. Angerstein-Kozlowska, B. E. Conway, B. Barnett, and J. Mozota, *J. Electroanal. Chem.*, **100**, 417 (1979).
43. K. J. Hanson and M. P. Green, *MRS Proc.*, **237**, 323 (1991).
44. F. Silva and A. Martins, *J. Electroanal. Chem.*, **467**, 335 (1999).